ISSN 1068-1620, Russian Journal of Bioorganic Chemistry, 2021, Vol. 47, No. 4, pp. 854–863. © The Author(s), 2021. This article is an open access publication.
Russian Text © The Author(s), 2021, published in Bioorganicheskaya Khimiya, 2021, Vol. 47, No. 4, pp. 495–505.

Derivative of Scorpion Neurotoxin BeM9 Is Selective for Insect Voltage-Gated Sodium Channels

M. A. Chernykh[a], N. A. Kuldyushev[a], S. Peigneur[b], A. A. Berkut[a], J. Tytgat[b], R. G. Efremov[a, c], A. A. Vassilevski[a, c, 1], and A. O. Chugunov[a, c]

[a] *Shemyakin–Ovchinnikov Institute of Bioorganic Chemistry, Russian Academy of Sciences, Moscow, 117997 Russia*
[b] *KU Leuven, ON II, Leuven, 3000 Belgium*
[c] *Moscow Institute of Physics and Technology (National Research University), Dolgoprudny, 141701 Russia*

Received October 1, 2020; revised October 23, 2020; accepted October 25, 2020

Abstract—Scorpion α-toxins are small proteins inhibiting the inactivation of voltage-gated sodium channels. They can selectively act on either mammalian (mammal toxins) or insect channels (insect toxins), or affect both types of channels (α-like toxins). Currently no model has been proposed that fully explains the dependence of selectivity upon amino acid sequence, but some patterns have already been established. Thus, most mammal toxins have an aspartic acid residue in position 8, which is involved in the formation of the nest motif, but it is still not clear whether this residue interacts directly with channels. The objective of our study was to obtain a derivative of the α-like toxin BeM9 with the replacement of lysine in position 8 by glutamate (K8E), changing the charge, but excluding the formation of the nest motif. In addition, we replaced the tyrosine in position 17 with glycine (Y17G), which is characteristic of mammal toxins. Surprisingly, the double-mutant derivative BeM9^{EG} lost its activity on mammalian channels, becoming an insect toxin. To explain these changes, we constructed models of BeM9 and BeM9^{EG} complexes with channels, and also performed molecular dynamics of isolated toxins. Analysis of intermolecular contacts in the complexes did not explain the reason for the selectivity change. Nevertheless, the structure of intramolecular contacts and data on molecular mobility indicate an important role of residues K8 and Y17 in stabilizing a certain conformation of BeM9 loops. We assume that the replacement of these residues allosterically affects the efficiency of toxin binding to channels.

Keywords: neurotoxins, voltage-gated sodium channels, protein engineering, molecular dynamics
DOI: 10.1134/S1068162021040063

INTRODUCTION

At present, novel compounds that can selectively affect targets in insect nervous system, such as voltage-gated sodium channels (VGSCs), are being developed. VGSCs are transmembrane proteins consisting of four homologous repeats (D I–IV). Each repeat comprises a voltage-sensing domain (VSD), which responds to changes in the transmembrane (TM) potential (TM helices S1–S4 and the loops between them). Two other helices (S5 and S6) from all repeats form a single pore domain (PD), which allows selective Na^+ permeation through the membrane. Activation of VSDs I–III is necessary to open the PD, whereas activation of VSD IV leads to a fast inactivation of the channels [1, 2].

Natural neurotoxins include modulators and blockers of ion channels, which are often proteins or peptides acting selectively on a particular type of channels in certain organisms. For example, the so-called "α-toxins" (α-NaTx) from scorpion venoms inhibit VGSC inactivation after binding to VSD IV (loops S1–S2 and S3–S4) and PD I (loop S5–S6) [3]. Some α-NaTx selectively affect mammalian channels (referred to as "mammal toxins"), others affect insect channels ("insect toxins"), and still others ("α-like toxins") have a wide spectrum of activity [4, 5]. Investigation of α-NaTx selectivity is important not only for fundamental science: specific insect toxins, apparently, can be used as insecticides, being safe for vertebrates [6].

In 2013, a comparative analysis of the molecular surface properties of the α-NaTx groups led to the hypothesis that primarily the "specificity module" determines their selectivity. This is a part of toxin formed by the N-terminal region (also called the "RT-loop"), β_2–β_3 loop, and the C-terminus attached to the N-terminal part by a disulfide bond (Fig. 1a) [7]. The structure of a complex of the mammal toxin Aah2

Abbreviations: PD, pore domain; VSD, voltage-sensing domain; VGSC, voltage-gated sodium channels; BeM9^{EG}, derivative of scorpion α-like toxin; α-NaTx, scorpion α-toxins.

[1] Corresponding author: e-mail: avas@ibch.ru.

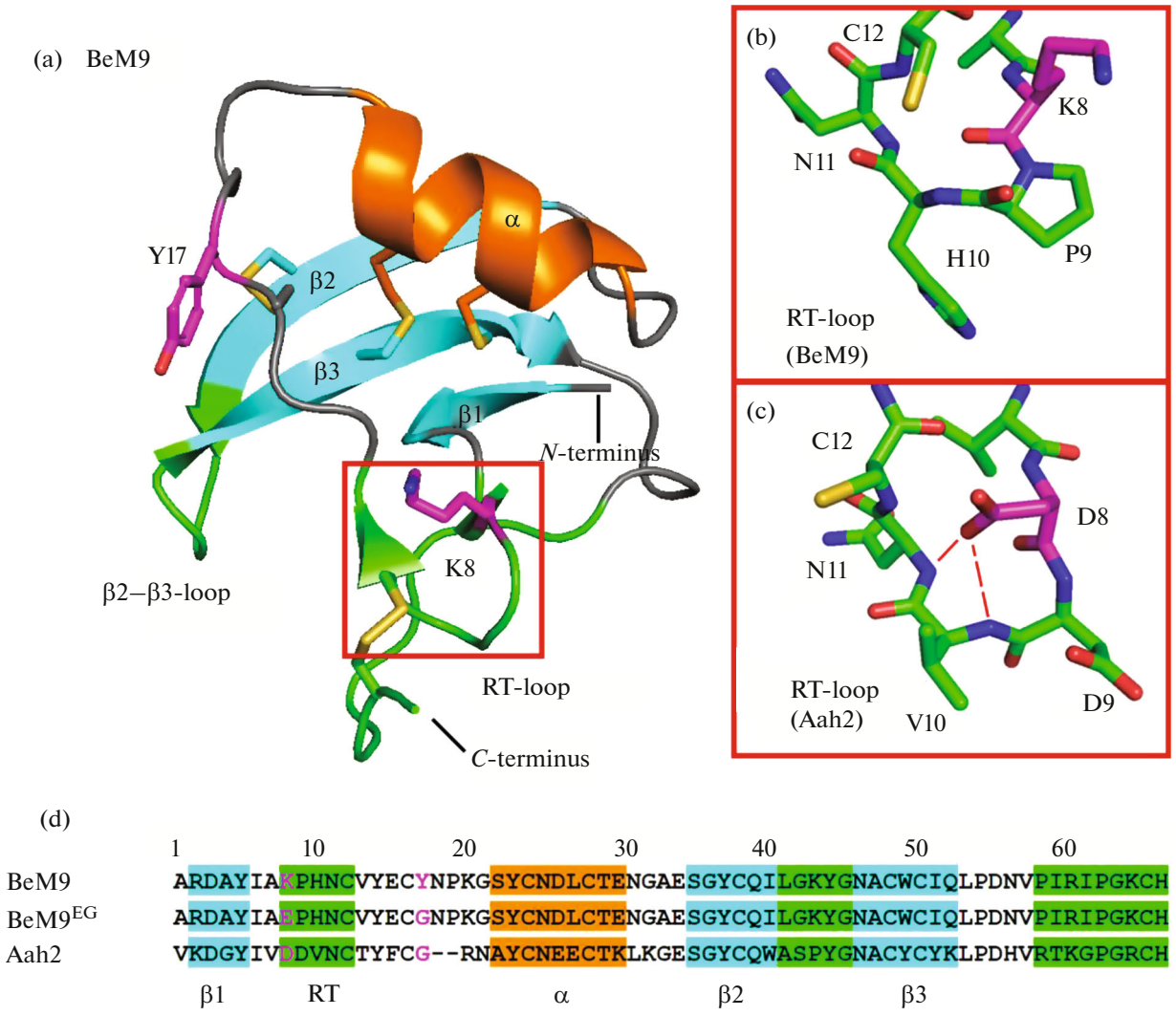

Fig. 1. α-NaTx structure. (a) Overall structure exemplified by the α-like toxin BeM9 (PDB ID: 5MOU [11]). According to the hypothesis [7], the specificity module consists of the RT-loop, β_2–β_3 loop and C-terminus (the rest of the molecule is called the core module) and is colored *green*; the three-stranded β-sheet (β_1–β_3) is in *blue*; the α-helix is *orange*; disulfide bridges are *yellow*; and mutated amino acid residues are *purple*. (b, c) The structures of the RT-loop in BeM9 and the typical mammal toxin Aah2 (PDB ID: 1PTX [14]). In Aah2, a "nest" motif is observed: the side chain of D8 is oriented inside the RT-loop and forms hydrogen bonds (*red dotted lines*) with V10 and N11 main-chain –NH groups, whereas in BeM9 K8 is oriented outwards and does not form such bonds. (d) Comparison of the amino acid sequences of BeM9, its double mutant $BeM9^{EG}$, and Aah2. Color code as in panel (a).

from the venom of the scorpion *Androctonus australis* with a chimeric VGSC, recently resolved with cryo-electron microscopy, shows that the specificity module actually forms contacts with the channel, while the rest of the toxin (its "core module") is not involved in the interaction [3].

α-Like toxin M9 (BeM9) from the venom of the scorpion *Mesobuthus eupeus* (formerly known as *Buthus eupeus*) is one of the most studied α-NaTx; its spatial structure was determined already in the 1980s at the Institute of Bioorganic Chemistry in Moscow and became the first studied structure of α-NaTx [8, 9]. We have previously used this α-NaTx to obtain a specific mammal toxin. For this, the specificity module of Aah2 was transferred onto the BeM9 framework; in addition, several amino acid residues of the core module were replaced [10]. A careful examination of BeM9 spatial structure revealed the key role of the R60 residue in the C-terminal region of the toxin. This residue organizes the specificity module with a network of hydrogen bonds which forms a special variant of the "niche" motif, referred to as "arginine hand" [11]. The R60K mutant lost the ability to interact with mammalian channels, thus becoming an insect toxin.

In this study, we focused on the role of another part of the specificity module (RT-loop; Fig. 1b) and

Table 1. Activity of BeM9 and its derivatives on VGSCs

Toxin	$Na_v1.2$	$Na_v1.4$	$Na_v1.5$	$Na_v1.6$	$BgNa_v1$
BeM9	n/a* (3)	0.23 ± 0.03 (4)	0.46 ± 0.03 (3)	0.60 ± 0.04 (8)	1.93 ± 0.05 (7)
$BeM9^E$	n/a (3)	n/a (4)	0.05 ± 0.01 (4)	0.05 ± 0.04 (3)	1.16 ± 0.03 (5)
$BeM9^{EG}$	n/a (3)	n/a (4)	n/a (4)	n/a (4)	0.56 ± 0.06 (6)

*n/a, no activity. The indicated values are $I_{30\ ms}/I_{min}$ or $I_{5\ ms}/I_{min}$ (for $Na_v1.5$; see explanations in Experimental). The mean values ± standard deviation are given, the number of independent experiments (*n*) is shown in parentheses.

obtained a new BeM9 derivative selective to insect VGSCs.

RESULTS AND DISCUSSION

Selection of Amino Acid Replacements for BeM9 Modification

Comparison of the amino acid sequences of α-NaTx reveals a highly conserved aspartic acid residue in position 8 of the RT-loop of mammal toxins. Insect toxins and α-like toxins usually have a neutral (Q) or positively charged residue (K, like in BeM9) in this position. Surprisingly, the classic insect toxin BjαIT from the venom of *Hottentotta judaicus* also has such aspartic acid residue, as in mammal toxins [12]. A careful structural analysis of α-NaTx revealed that in mammal toxins this residue preserves a certain conformation of the RT-loop via formation of several hydrogen bonds with –NH groups of the main chain (a so-called "nest" motif [13], Fig. 1c). We decided to find out whether the negative charge of the residue in position 8 directly affects the interaction with mammalian channels. In order to prevent the formation of the nest motif, we replaced K8 in BeM9 with not aspartic but glutamic acid residue, the side chain of which is too long to form the motif.

As it was found earlier [7], the RT-loop in mammal toxins is characterized by relatively high mobility. It is partially explained by the presence of the glycine residue G17 (Aah2 numbering) typical for mammal toxins at the site connecting the RT-loop with the α-helix. Based on the analysis of amino acid sequences and the spatial structure of α-NaTx, we assumed that changes in the charge and mobility of the RT-loop due to two mutations (K8E and Y17G, see Fig. 1d), would switch the specificity of α-like toxin BeM9 to mammalian channels. To test this assumption, we produced recombinant BeM9 derivatives.

Production of Recombinant BeM9 and Its Derivatives

To obtain material for the studies of activity, we used a bacterial expression system and the plasmid encoding BeM9 produced in a previous study [7, 11]. DNA encoding BeM9-K8E ($BeM9^E$) and BeM9-K8E, Y17G ($BeM9^{EG}$) was obtained with PCR from overlapping synthetic oligonucleotides. The genes of the target polypeptides were cloned in one ORF with the carrier protein thioredoxin (Trx). Fusion proteins Trx-BeM9, Trx-$BeM9^E$ and Trx-$BeM9^{EG}$ were isolated from the total bacterial cell lysate using metal-chelate affinity chromatography. The target polypeptides were cleaved from Trx using cyanogen bromide. The chromatographic purity of the obtained polypeptides (>95%) was achieved after two rounds of HPLC.

The correct synthesis of the target polypeptides with the formation of disulfide bonds was confirmed by measuring of the molecular mass of the purified products BeM9, $BeM9^E$, and $BeM9^{EG}$ by MALDI mass spectrometry. The measured masses were 7335.1, 7336.1, and 7230.1 Da, respectively (calculated masses are 7335.2, 7336.2, and 7230.0 Da); the yield was 2 mg per 1 liter of LB medium. The correct formation of disulfide bonds is a significant problem in heterologous expression of proteins. In the case of BeM9 and its derivatives, this problem was solved by using Trx: it is known that it promotes correct folding of disulfide-containing proteins [15]. The spatial structure of the recombinant BeM9 recently solved using NMR spectroscopy, confirms the correct formation of S–S bridges [11].

BeM9 Derivatives Activity Measurements on VGSCs

The effects of the BeM9 derivatives on VGSCs were compared to the parent toxin at the concentration of 1 μM. We used a standard approach with the expression of channel genes (α-subunits and corresponding auxiliary β-subunits) in *Xenopus laevis* oocytes (Fig. 2). As the original toxin, $BeM9^E$ and $BeM9^{EG}$ showed no activity on $Na_v1.2$ but were active on the cockroach channel $BgNa_v1$, although the activity became less pronounced (Table 1). In contrast to BeM9, $BeM9^E$ was strikingly less active on $Na_v1.5$ and $Na_v1.6$, while $BeM9^{EG}$ showed no activity on these channels at all. Thus, $BeM9^{EG}$ was not active on any mammalian channels tested and was classified as an insect toxin.

Models of Complexes with Channels Do Not Explain BeM9 and $BeM9^{EG}$ Specificity

The spatial structure of a complex of the mammal toxin Aah2 with the chimeric channel $hNa_v1.7$-

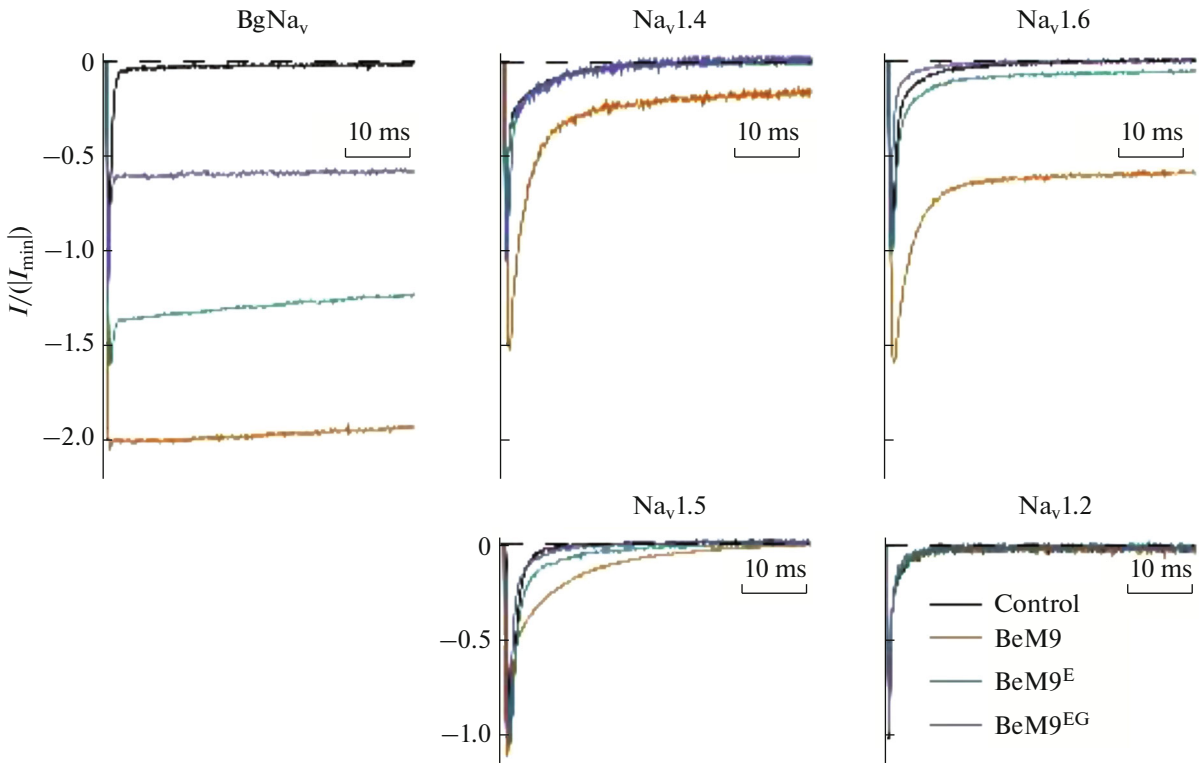

Fig. 2. Activity of BeM9 and its derivatives on VGSC isoforms. Currents through membranes of oocytes expressing cloned isoforms of VGSCs in control and after incubation with toxins at 1 μM concentration. The *dotted line* indicates the zero current level. The current amplitude is given in arbitrary units $I/(|I_{min}|)$ (see explanations in Experimental). Representative records of at least three independent experiments are provided.

Na$_v$Pas was determined in 2019 (PDB ID: 6NT4 [3]). In this chimeric channel, fragments of the Na$_v$Pas channel from the cockroach *Periplaneta americana*, including extracellular loops of VSD IV and the contacting region of PD I, were replaced with the corresponding sequences of the human channel Na$_v$1.7. We hypothesized that the models of BeM9 complexes with mammalian and insect VGSCs based on this spatial structure would be able to explain the nature of BeM9^{EG} selectivity. Static models of BeM9 and BeM9^{EG} were built in complex with human Na$_v$1.4 and cockroach BgNa$_v$ channels (Fig. 3), and intermolecular contacts in the models were investigated (see Experimental for details of the modeling). We expected to see a clear change in the intermolecular contacts, explaining the loss of BeM9^{EG} affinity to mammalian channels, but the results of the simplistic modeling did not show this. According to the model, the Y17/G17 residues do not contact with the channel and cannot directly affect the toxin activity. K8 in BeM9 does not interact with the channels either, while in BeM9^{EG} E8 forms an intermolecular ionic bond with the K1439/1705 residue (numbering for hNa$_v$1.4/BgNa$_v$) (Figs. 3c, 3d). BeM9 also interacts with K1439/1705, but using another residue, i.e. E15.

The analysis of the complexes does not explain the selectivity change in BeM9^{EG}, since the structure of the S3–S4 loop is highly conserved. We supposed that the reason for that phenomenon were allosteric effects. This led us to the analysis of changes in the structure and intramolecular contacts of the mutated toxin.

Analysis of BeM9 Structural Changes Caused by Mutations

Since we could not explain the changes in the specificity by using the "static" models of the BeM9/VGSC complexes, we decided to study the dynamic properties of BeM9 and its derivative BeM9^{EG}. For each of the molecules, we performed molecular dynamics (MD) simulations with a length of 100 ns in triplicate. We searched structural changes by analyzing the intramolecular contacts such as hydrogen bonds, hydrophobic interactions, ionic bonds, stacking and cation–π interactions, which were presented with contact maps (66 × 66 point arrays; Fig. 4).

The analysis of the intramolecular contacts and the root mean square fluctuations (RMSF) showed that one of the mutations (Y17G) increases the mobility of the loop preceding the α-helix due to a loss of the

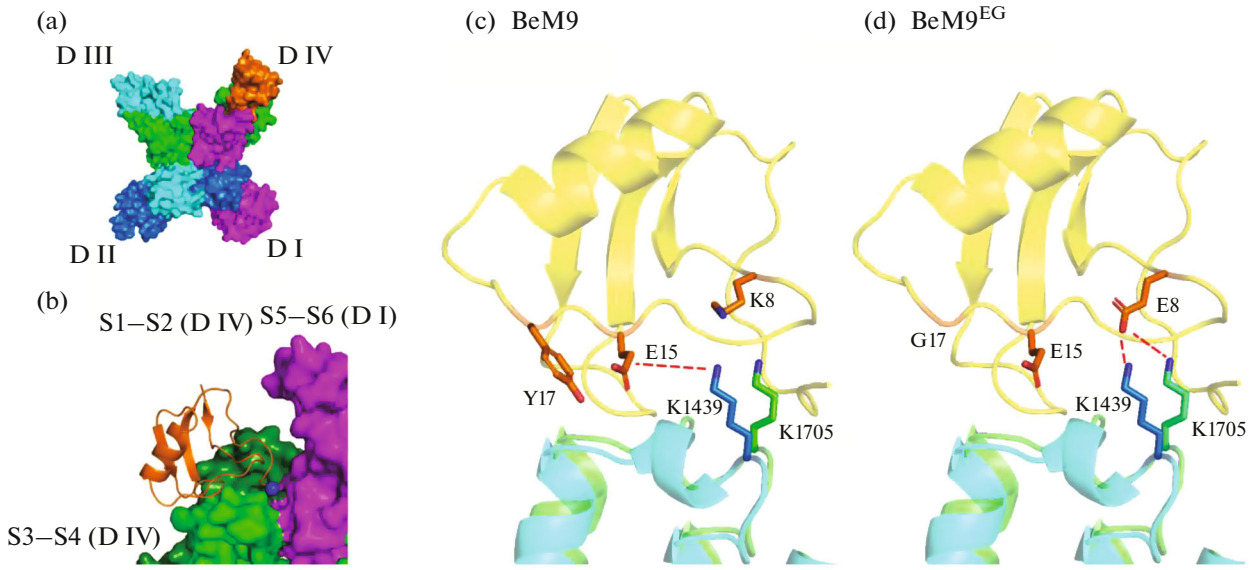

Fig. 3. Modeled complexes of VGSCs with BeM9 and its mutant BeM9^{EG}. (a) General view of the complex of VGSC with α-NaTx from the extracellular side. VGSC is depicted as a *colored surface* with individually colored homologous repeats: D I (*purple*), D II (*dark blue*), D III (*light blue*), and D IV (*green*). The centrally located parts of each repeat form the PD; the distal parts form VSDs I–IV. The toxin (shown in *orange*) binds to the channel in the area of VSD IV, partially capturing PD I. (b) The toxin binding site (enlarged). The S3–S4 loop is colored in *light green*, S1–S2 in *dark green*, PD I in *purple*, and the C-terminus of the toxin is marked with a *blue sphere*. (c, d) Ionic bonds between the RT-loop of BeM9 and the S3–S4 loop of VGSCs. The toxin molecule is shown in *yellow* (BeM9 in panel C and BeM9^{EG} in panel d), $Na_v1.4$ is in *blue*, and $BgNa_v$ is in *green*. Key amino acid residues of the toxin involved in the interaction with channels or subject to mutagenesis are colored in *orange*.

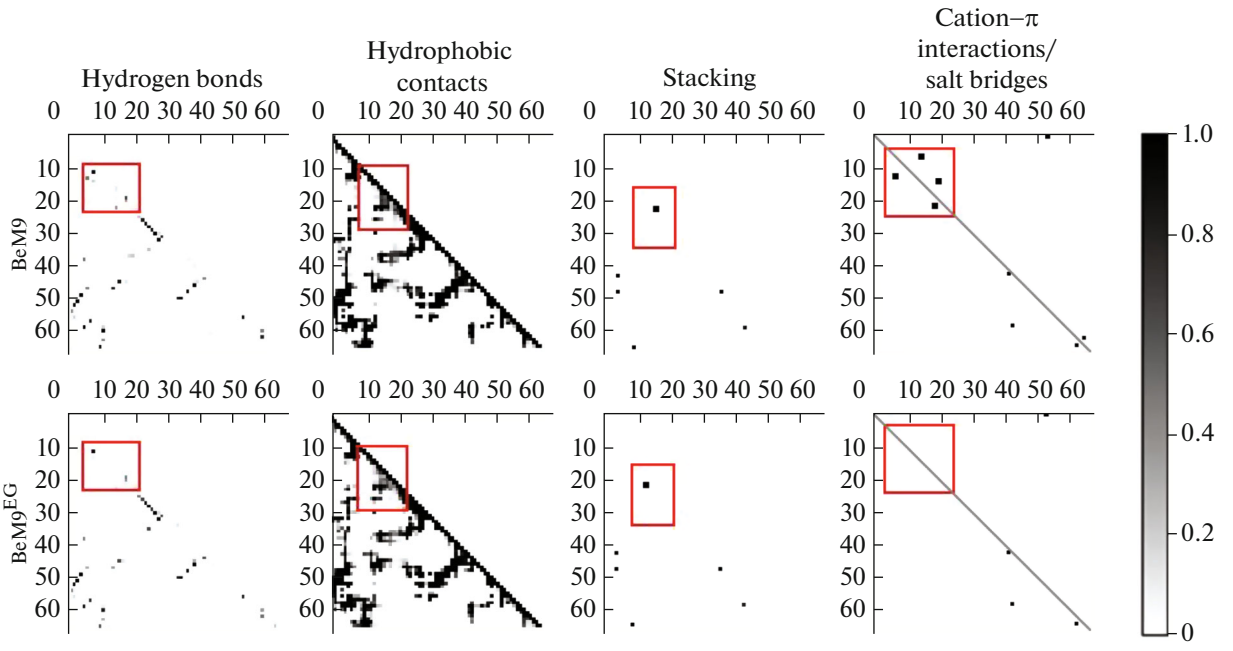

Fig. 4. Intramolecular contact maps for BeM9 and BeM9^{EG}. The coordinates of each point correspond to the numbers of residues that may contact each other. The color intensity of the points for hydrogen bonds and hydrophobic contacts (see the scale to the right) shows the contact lifetime (as a fraction of the total duration of three MD trajectories (3 × 100 ns)). Other types of contacts are shown qualitatively: only contacts with >10% lifetime are shown. Contacts located near the RT-loop are outlined in *red* and are represented by *larger dots*. Contacts of BeM9 are shown in the upper row, and those for BeM9^{EG} are in the lower row. The regions of the most significant difference between BeM9 and BeM9^{EG} reflecting the effects of K8E and Y17G mutations are marked with *red boxes*. For cation–π interactions and ionic bonds, a single map is shown: ionic bonds are plotted above the diagonal, and cation–π interactions are below the diagonal.

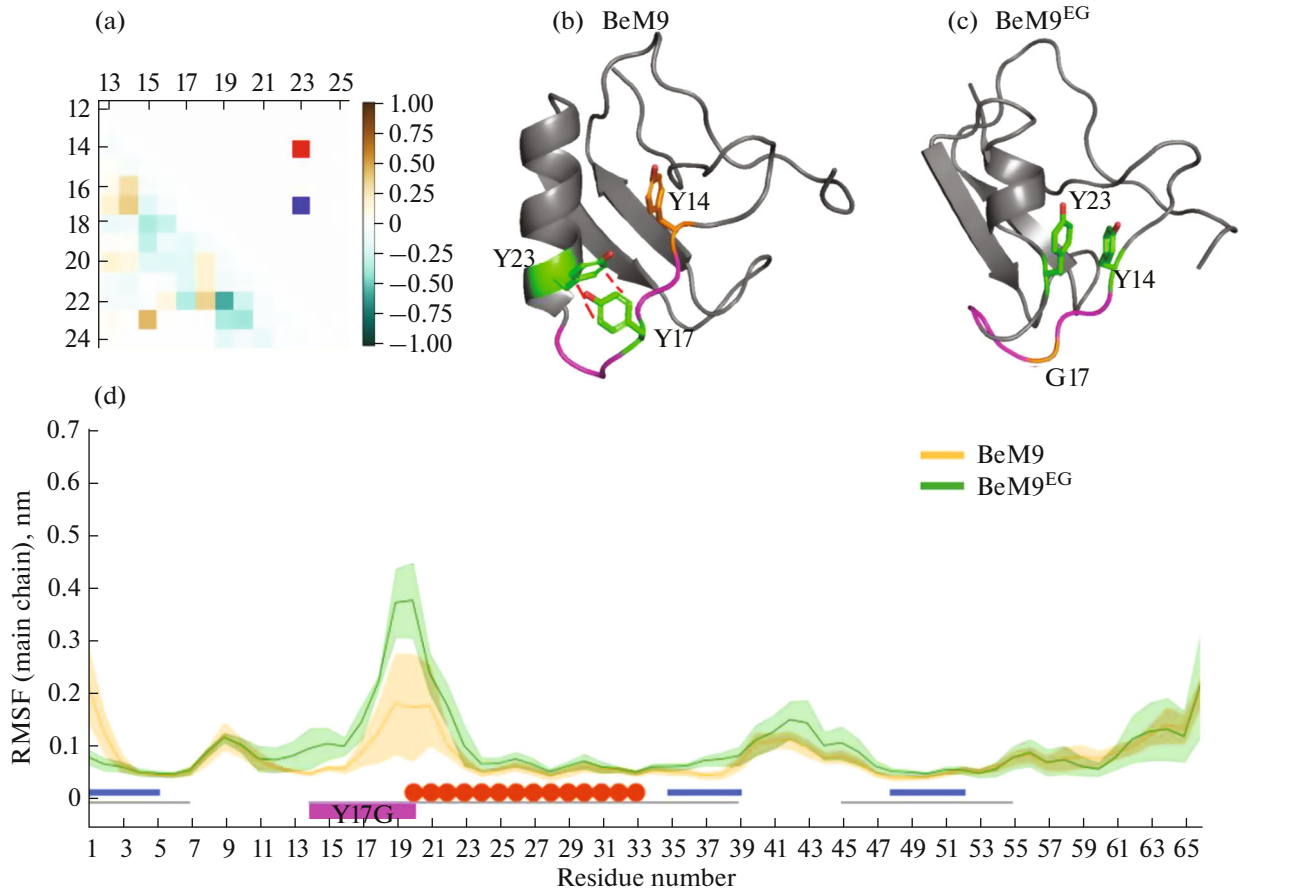

Fig. 5. Influence of the Y17G mutation on BeM9 structure. (a) Differential map of contacts between BeM9 and BeM9^{EG} near the RT-loop and the α-helix. The map was obtained by subtracting the maps of hydrophobic (lower left part of the map) and stacking contacts (upper right part) in BeM9 from BeM9^{EG} (Fig. 4). *Blue* shows the loss of hydrophobic contacts in BeM9^{EG} compared to BeM9, and *brown* depicts the gain of contacts (according to the scale on the right). *Blue square* shows the loss of the Y17–Y23 stacking interaction in BeM9, and *red square* shows the formation of the Y14–Y23 stacking interaction in BeM9^{EG}. Panels b, c show typical conformations selected from MD calculations. (b) BeM9 structure. The residues involved in stacking contacts are in *green*; residues not involved in this structure, but involved in BeM9^{EG} are in *orange*; residues with increased mobility after mutation are in *purple*; and all other residues are in *gray*. (c) BeM9^{EG} structure. *Green* shows residues involved in stacking contacts in BeM9^{EG}, and *orange* indicates residues that are not involved in stacking interactions in BeM9^{EG}, but are involved in such interactions in BeM9. (d) RMSF values for BeM9 (*yellow*) and BeM9^{EG} (*green*), averaged over three trajectories. The *gray line* under the graph corresponds to the core module, β-strands are colored in *blue*, the α-helix in *red*, and the vicinity of the Y17G substitution, where mobility increases after mutation (the same area as in panels b, c) is in *purple*.

hydrophobic interactions and Y17–Y23 stacking as well as an increase of main chain flexibility due to the substitution to a glycine residue. The newly formed Y14–Y23 contact in BeM9^{EG}, apparently, does not have a stabilizing effect on this part of the toxin. The key effects of the Y17G mutation are illustrated in Fig. 5.

The impact of the key mutation K8E is the reorganization of a system of ionic bonds and cation–π interactions (Fig. 6). The nest motif, as expected, was not observed in the mutant (Fig. 6b). Moreover, K8 in BeM9 formed stable contacts K8–Y14 and K8–E15, which are destroyed due to reversal of charge and repulsion between E8 and E15. Also, the mutant lost the E15–K20 contact, which can be explained by the effects of both substitutions. K8 can balance between Y14 and E15, and E15 can switch between K8 and K20, representing two stable BeM9 conformations, whereas BeM9^{EG} is generally more mobile and less ordered.

EXPERIMENTAL

Preparation of Recombinant BeM9 Derivatives

Nucleotide sequences encoding BeM9^{E} and BeM9^{EG} were synthesized using ligation of oligonucleotides (Table 2) and PCR as described for BeM9 [7, 16]. The resulting full-length sequences were cloned into the expression vector pET-32b (Novagen) using the KpnI and BamHI restriction sites. The obtained

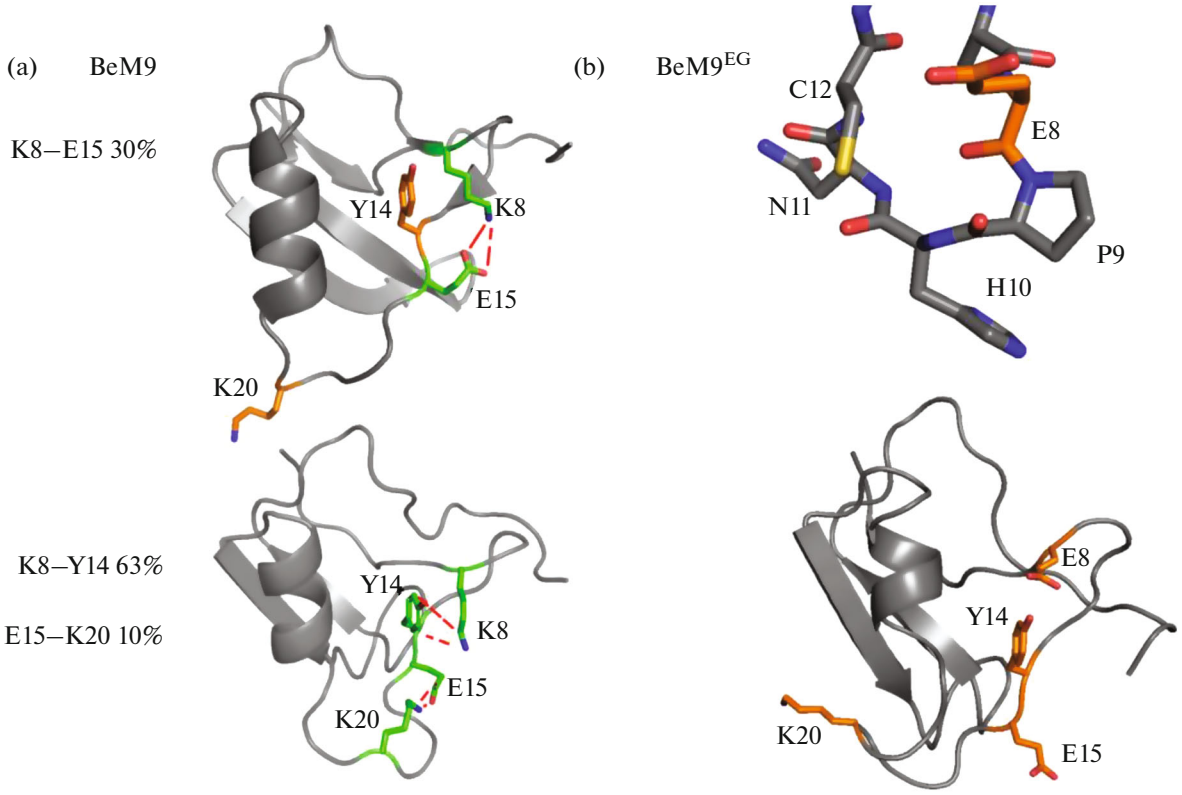

Fig. 6. Effect of the K8E mutation on BeM9 structure. K8, Y14, E15 and K20 residues, participating in ionic and cation–π interactions, are shown in *green*, the same residues that are not participating in such interactions are in *orange*, and other residues are in *gray*. The *red dotted lines* show interactions between residues. The presented conformations are taken from MD calculations. (a) Structure of BeM9. The top panel shows the K8–E15 ionic bond, and the bottom panel shows the E15–K20 ionic bond and the K8–Y14 cation–π interaction. To the left of the structures, the lifetimes are shown for the corresponding contacts, averaged over three trajectories. (b) $BeM9^{EG}$ structure. The top panel shows the structure of the RT-loop similar to Figs. 1b, 1c. Below is a general view of the structure.

chimeric genes of fusion proteins consisted of Trx and the toxin: Trx-$BeM9^{E}$ and Trx-$BeM9^{EG}$.

The chimeric genes were expressed in *Escherichia coli* BL21 (DE3) strain [17]. Bacteria transformed with an expression vector were cultured in the LB medium supplemented with ampicillin (100 μg/mL) at 37°C and with vigorous stirring. The expression of the target genes was induced by adding 0.2 mM isopropyl-β-D-1-thiogalactopyranoside to the medium, and the culture was incubated for another 4 h. After that, bacteria were precipitated, resuspended in the starting buffer for affinity chromatography (300 mM NaCl, 20 mM Tris-HCl, pH 7.5) and lysed by ultrasonication.

The fusion proteins contained a hexahistidine sequence to purify them using metal chelate affinity chromatography [18] on a TALON Superflow Metal Affinity Resin sorbent (Clontech). The sorbed proteins were eluted with an imidazole buffer (150 mM imidazole, 300 mM NaCl, 20 mM Tris-HCl, pH 7.5). BeM9 derivatives do not contain methionine residues; therefore, the target toxins were cleaved from Trx using cyanogen bromide as described [19]. To do so, a methionine codon was introduced into the sequence of chimeric genes immediately before the toxin gene. The BeM9 derivatives cleaved from Trx were purified by reversed-phase HPLC.

Mass Spectrometry

Polypeptides were analyzed using MALDI time-of-flight mass spectrometry. We used an Ultraflex TOF-TOF spectrometer (Bruker Daltonik), the analysis was performed as described previously [20] using 2,5-dihydroxybenzoic acid (Sigma-Aldrich) as a matrix. The measurements were carried out in both linear and reflector modes. Mass spectra were analyzed using Data Analysis 4.3 and Data Analysis Viewer 4.3 software (Bruker).

Electrophysiology

The activity of the obtained derivatives was compared to the parent BeM9 toxin based on the effect on VGSC expressed in *X. laevis* oocytes. Isolation of frog

Table 2. Sequence of synthetic oligonucleotides used to construct DNA encoding BeM9 derivatives

Name	Sequence
M9f1	ATAT*GGTACCATG*GCTCGTGACGCTTACATCGCTG
M9f2*	AACCGCACAACTGCGTTTACGAATGCTACAACCCGAAAGGTTCTT
M9f2-2*	AACCGCACAACTGCGTTTACGAATGCGGCAACCCGAAAGGTTCTT
M9f3	ACTGCAACGACCTGTGCACCGAAAACGGTGCTGAATCTGGTTACT
M9f4	GCCAGATCCTGGGTAAATACGGTAACGCTTGCTGGTGCATCCA
M9f5	GCTGCCGGACAACGTTCCGATCCGTATCCCGGGTAAATGCC
M9r1/2	AAACGCAGTTGTGCGGTTCAGCGATGTAAGCGTCAC
M9r2/3*	TGCACAGGTCGTTGCAGTAAGAACCTTTCGGGTTGT
M9r2/3-2*	TGCACAGGTCGTTGCAGTAAGAACCTTTCGGGTTGC
M9r3/4	ATTTACCCAGGATCTGGCAGTAACCAGATTCAGCAC
M9r4/5	GAACGTTGTCCGGCAGCTGGATGCACCAGCAAGC
M9r	GCAT*GGATCC***CTA**GTGGCATTTACCCGGGATAC

Restriction sites (KpnI in M9f1 and BamHI in M9r) are in italics, the methionine codon is in bold type and italics, the stop codon is in bold. Nucleotides that differ from the sequence of the BeM9 gene are underlined.

* M9f2 and M9r2/3 was used for the synthesis of the $BeM9^{E}$ gene, and M9f2-2 and M9r2/3-2 were used for $BeM9^{EG}$.

oocytes, RNA preparation, data collection and analysis were performed as described previously [7, 10]. We used genes of mammalian VGSC isoforms: rat (r)$Na_v1.2$ and 1.4, human (h)$Na_v1.5$, murine (m)$Na_v1.6$, auxiliary rβ1 and hβ1 subunits, as well as $BgNa_v1$ α-subunit cloned from the cockroach *Blattella germanica* and TipE auxiliary subunit from *Drosophila melanogaster*. To assess the efficacy of toxins, we divided the value of the recorded current through the oocyte membrane 30 ms after the test pulse by the peak current ($I_{30\ ms}/I_{min}$). In the case of the $Na_v1.5$ channel, due to its fast kinetics, the value of the current 5 ms after the test pulse was divided by the peak current ($I_{5\ ms}/I_{min}$). All data were analyzed using pClamp Clampfit software version 10.4 (Molecular Devices) and Origin Pro version 8.0 (OriginLab).

Molecular Modeling

For comparative analysis we modeled complexes of BeM9 and $BeM9^{EG}$ toxins with human $Na_v1.4$ and cockroach $BgNa_v$. The template for modeling was the complex of the chimeric channel $hNa_v1.7$-Na_vPas with Aah2 (PDB ID: 6NT4 [3]), Aah2 was replaced by the studied toxin via spatial alignment, and $hNa_v1.7$-Na_vPas was analogously replaced by the studied channel. $hNa_v1.4$ and $BgNa_v$ models were constructed using homology modeling in MODELLER v. 9.19 [21] based on the $hNa_v1.7$-Na_vPas template. To minimize the energy of the complexes, vacuum cubic cells ($160 \times 160 \times 160$ Å^3) were used. For this, we utilized GROMACS 5.1.2 [22] and the amber99sb-ildn.ff force field [23]. Intramolecular effects of mutations in BeM9 were assessed by comparative modeling of the wild-type α-like toxin BeM9 (PDB ID: 5MOU) and its double mutant $BeM9^{EG}$ specific for insect VGSCs, which was modeled using MODELLER.

MD was used to compare the intrinsic dynamics of molecules. The cutoff radii of van der Waals and electrostatic interactions were 10 and 12 Å, respectively. For MD of the toxins, cubic cells ($55 \times 55 \times 55$ Å^3) were constructed using the SPC water model [24], containing counterions for electroneutrality and heated to 300 K for 100 ps. MD was carried out under periodic boundary conditions at $T = 300$ K, $P = 1$ bar employing the V-rescale thermostat [25] and Berendsen barostat [26]. The length and step of the trajectory were 100 ns and 2 fs, respectively. For each studied molecule, three MD runs were performed to accumulate statistics.

Molecular Contacts

Intra- and intermolecular contacts were calculated using IMPULSE software (developed by N.A. Krylov, in preparation for publication). All pairwise interactions found in the trajectories were classified as hydrogen bonds, hydrophobic contacts, ionic bonds, parallel and T-shaped stacking based on mutual arrangement, interaction energy, and type of contacting residues. The data were converted into the format of point maps with 66×66 size, where each coordinate corresponds to the residues number, and the color intensity reflects the contact lifetime (0–100% of 100 ns), using our own Python script.

CONCLUSIONS

In this work we tried to clarify the mechanism behind the observed selectivity change of the α-like toxin BeM9 after introducing two substitutions (K8E

and Y17G) into its structure. These mutations led to an unexpected result: BeM9^{EG} lost activity on mammalian channels and remained active on insect channels, whereas we expected the opposite. We compared the models of complexes of mammalian and insect VGSCs with BeM9 and BeM9^{EG} and performed a comparative analysis of intramolecular contacts in these toxins using MD.

Analysis of the complexes with the VGSCs revealed what had changed: the K1439/1705 residue of the channels forms an ionic bond with E15 in BeM9, while K8 does not participate in this interaction. At the same time, E8 residue of BeM9^{EG} contacts K1439/1705. However, the S3–S4 loop and, in particular, the K1439/1705 residue are conserved; therefore, our models could explain the total activity change (towards all VGSC subtypes) but not the change in the toxin selectivity. We conclude that such simple models of complexes are not informative. The reason for the selectivity change may be allosteric effects.

Analysis of the MD of isolated toxins revealed that the fragment in the vicinity of the Y17G substitution in BeM9^{EG} has a higher mobility. This can be explained by the loss of the Y17–Y23 stacking contact as well as by the flexibility of the backbone in the region due to the glycine residue. The K8E replacement destroys the switchable system of bonds K8–E15–K20 and Y14–K8–E15, which can decrease the stability of the RT-loop and its environment. In BeM9^{EG}, these contacts are lost, consequently, the RT-loop and its vicinity become more mobile, and the system of two stable conformations (with ionic bonds K8–E15 and E15–K20) disappears. We assume that such rearrangement of the toxin resulting from the mutagenesis destabilizes the complex with mammalian VGSCs. Further detailed study of the structure and conformational dynamics of the specificity module of α-NaTx can reveal the nature of the "double" activity of α-like toxins and facilitate the creation of selective ligands for various types of VGSC.

FUNDING

This work was supported by the Russian Science Foundation (grant no. 20-44-01015). J. Tytgat is grateful to the Research Foundation—Flanders (FWO, grants G0C2319N, G0A4919N, and G0E7120N). S. Peigneur was supported by KU Leuven (PDM/19/164).

COMPLIANCE WITH ETHICAL STANDARDS

This article does not include research involving human subjects.

All manipulations with frogs were carried out in accordance with the principles of ARRIVE (Animal Research: Reporting of In Vivo Experiments) and the European Convention for the Protection of Vertebrate Animals used for Experimental and Other Scientific Purposes (Strasbourg, March 18, 1986).

Conflict of Interests

The authors declare no conflicts of interest.

OPEN ACCESS

REFERENCES

1. Catterall, W.A., *Neurochem. Res.*, 2017, vol. 42, pp. 2495–2504. https://doi.org/10.1007/s11064-017-2314-9
2. Capes, D.L., Goldschen-Ohm, M.P., Arcisio-Miranda, M., Bezanilla, F., and Chanda, B., *J. Gen. Physiol.*, 2013, vol. 142, pp. 101–112. https://doi.org/10.1085/jgp.201310998
3. Clairfeuille, T., Cloake, A., Infield, D.T., Llongueras, J.P., Arthur, C.P., and Li, Z.R., *Science*, 2019, vol. 363, no. 6433. https://doi.org/10.1126/science.aav8573
4. Bosmans, F. and Tytgat, J., *Toxicon*, 2007, vol. 49, pp. 142–158. https://doi.org/10.1016/j.toxicon.2006.09.023
5. Gordon, D., Karbat, I., Ilan, N., Cohen, L., Kahn, R., and Gilles, N., *Toxicon*, 2007, vol. 49, pp. 452–472. https://doi.org/10.1016/j.toxicon.2006.09.023
6. King, G.F., *Pest Manage. Sci.*, 2019, vol. 75, pp. 2437–2445. https://doi.org/10.1016/j.toxicon.2006.11.016
7. Chugunov, A.O., Koromyslova, A.D., Berkut, A.A., Peigneur, S., Tytgat, J., and Polyansky, A.A., *J. Biol. Chem.*, 2013, vol. 288, pp. 19014–19027. https://doi.org/10.1002/ps.5452
8. Pashkov, V.S., Anh, Hoang, N., Maiorov, V.N., and Bystrov, V.F., *Peptides*, 1988, pp. 77–78. https://doi.org/10.1074/jbc.M112.431650
9. Pashkov, V.S., Khoang, N.A., Maiorov, V.N., and Bystrov, V.F., *Bioorg. Khim.*, 1986, vol. 12, pp. 1306–1316. https://doi.org/10.1007/978-94-010-9595-2_21
10. Kuldyushev, N.A., Berkut, A.A., Peigneur, S., Tytgat, J., Grishin, E.V., and Vassilevski, A.A., *FEBS Lett.*,

2017, vol. 591, pp. 3414–3420.
https://doi.org/10.1002/1873-3468.12839

11. Kuldyushev, N.A., Mineev, K.S., Berkut, A.A., Peigneur, S., Arseniev, A.S., and Tytgat, J., *Proteins*, 2018, vol. 86, pp. 1117–1122.
https://doi.org/10.1002/prot.25583
12. Arnon, T., Potikha, T., Sher, D., Elazar, M., Mao, W., and Tal, T., *Insect Biochem. Mol. Biol.*, 2005, vol. 35, pp. 187–195.
https://doi.org/10.1016/j.ibmb.2004.11.005
13. Watson, J.D. and Milner-White, E.J., *J. Mol. Biol.*, 2002, vol. 315, pp. 171–182.
https://doi.org/10.1006/jmbi.2001.5227
14. Housset, D., Habersetzer-Rochat, C., Astier, J.P., and Fontecilla-Camps, J.C., *J. Mol. Biol.*, 1994, vol. 238, pp. 88–103.
https://doi.org/10.1006/jmbi.1994.1270
15. LaVallie, E.R., DiBlasio, E.A., Kovacic, S., Grant, K.L., Schendel, P.F., and McCoy, J.M., *Biotechnology*, 1993, vol. 11, pp. 187–193.
https://doi.org/10.1038/nbt0293-187
16. Shlyapnikov, Y.M., Andreev, Y.A., Kozlov, S.A., Vassilevski, A.A., and Grishin, E.V., *Protein Expr. Purif.*, 2008, vol. 60, pp. 89–95.
https://doi.org/10.1016/j.pep.2008.03.011
17. Stüdier, F.W. and Moffatt, B.A., *J. Mol. Biol.*, 1986, vol. 189, pp. 113–130.
https://doi.org/10.1016/0022-2836(86)90385-2
18. Hochuli, E., Bannwarth, W., Dobeli, H., Gentz, R., and Stüber, D., *Nat. Biotechnol.*, 1988, vol. 6, pp. 1321–1325.
https://doi.org/10.1038/nbt1188-1321
19. Andreev, Y.A., Kozlov, S.A., Vassilevski, A.A., and Grishin, E.V., *Anal. Biochem.*, 2010, vol. 407, pp. 144–146.
https://doi.org/10.1016/j.ab.2010.07.023
20. Kuzmenkov, A.I., Sachkova, M.Y., Kovalchuk, S.I., Grishin, E.V., and Vassilevski, A.A., *Biochem. J.*, 2016, vol. 473, pp. 2495–2506.
https://doi.org/10.1042/BCJ20160436
21. Webb, B. and Sali, A., *Curr. Protoc. Bioinform.*, 2016, vol. 54, p. 37.
https://doi.org/10.1002/cpbi.3
22. Abraham, M.J., Murtola, T., Schulz, R., Pall, S., Smith, J.C., and Hess, B., *SoftwareX*, 2015, vols. 1–2, pp. 19–25.
https://doi.org/10.1016/j.softx.2015.06.001
23. Lindorff-Larsen, K., Piana, S., Palmo, K., Maragakis, P., Klepeis, J.L., and Dror, R.O., *Proteins*, 2010, vol. 78, pp. 1950–1958.
https://doi.org/10.1002/prot.22711
24. Jorgensen, W.L., Chandrasekhar, J., Madura, J.D., Impey, R.W., and Klein, M.L., *J. Chem. Phys.*, 1983, vol. 79, pp. 926–935.
https://doi.org/10.1063/1.445869
25. Bussi, G., Donadio, D., and Parrinello, M., *J. Chem. Phys.*, 2007, vol. 126, p. 014101.
https://doi.org/10.1063/1.2408420
26. Berendsen, H.J.C., Postma, J.P.M., van Gunsteren, W.F., DiNola, A., and Haak, J.R., *J. Chem. Phys.*, 1984, vol. 81, pp. 3684–3690.
https://doi.org/10.1063/1.448118